Linear analysis of a three-dimensional rectangular Cerenkov maser with a sheet electron beam*

Chen Ye(陈 晔)[a)b)†], Zhao Ding(赵 鼎)[a)], and Wang Yong(王 勇)[a)]

[a)] *Key Laboratory of High Power Microwave Sources and Technologies, Institute of Electronics, Chinese Academy of Sciences, Beijing* 100190, *China*

[b)] *Graduate University of the Chinese Academy of Sciences, Beijing* 100049, *China*

(Received 29 March 2011; revised manuscript received 12 May 2011)

A linear theory of a rectangular Cerenkov maser (RCM) with a sheet electron beam is developed by using the field-match method. Based on the three-dimensional beam-wave interaction model proposed in this paper, a hybrid-mode dispersion equation and its analytical solution are derived for the RCM. Through numerical calculations, the effects of the beam-grating gap, beam thickness, current density, beam voltage and waveguide width on the linear growth rate are analysed. Moreover, the performance difference between the RCM with the closed transverse boundary and that with the upper open boundary is compared. The results show that the closed RCM model can avoid the effect of RF radiation on beam-wave interaction, which is more rational for practical applications.

Keywords: Cerenkov maser, field-match method, beam-wave interaction, hybrid-mode dispersion, growth rate

PACS: 84.40.Ik, 94.05.Pt, 41.60.Bq, 41.20.Jb **DOI:** 10.1088/1674-1056/20/10/108402

1. Introduction

The research on Cerenkov masers can be dated back to the late 1940s. From then on, a series of remarkable theoretical and experimental results has been reported.[1−9] Cerenkov masers, characterized by high power and high frequency coherent radiation and a wide tunable range of working frequency, have become one of the most promising candidates to produce high power millimeter-waves or microwaves, which have potential applications in radar, communication systems and plasma heating.

For practical Cerenkov masers (CM), there are two possible structures. One is a cylindrical Cerenkov maser (CCM) and the other is a rectangular Cerenkov maser (RCM). The CCM adopts a cylindrical waveguide as the interaction structure, where an annular electron beam interacts with the TM_{on} modes. In the 1990s, a CCM produced megawatt-level peak and/or kilowatt-level average powers in the centimeter-wave regime with a efficiency of 30%–50%.[5,6,10−13] However, the geometrical scale of the practical device is always analogous to the working wavelength, so the operation of a CCM for high power levels is limited when the wavelength becomes short. Moreover, in order to keep a proper shape and position of the beam for the beam–wave interaction, and to avoid the beam deformation and the boundary interception of the beam resulting from the high current density in the hollow beam, a strong axial magnetic field must be applied, which commonly needs large focusing equipment. An RCM with a sheet beam adopts a rectangular waveguide with a loaded dielectric layer or metal slow-wave structure, in which the RF field interacts with a sheet beam. Compared with the conventional CM, the focusing of the beam in the RCM can be realized using periodic permanent magnets, because of the smaller space-charge force in the sheet beam. In the RCM, a transverse size of the sheet beam can be enlarged to improve the power capability and reduce space-charge force, while the other size remains small and compatible with the millimeter-wave operation.

Some work on the RCM was done in the early 1990s, when the researchers in the University of Wisconsin derived a hybrid-mode dispersion equation for a dielectric loaded RCM with a sheet beam, in which the analytic results for growth rates, bandwidth and mode competition in the limit of a dilute beam are presented.[14] In the early 2000s, Calsten has put forward a conceptual design of the RCM that was used in a low-frequency communication system.[15] According

*Project supported by the National Natural Science Foundation of China (Grant No. 60801031).

†Corresponding author. E-mail: chenye07@mails.gucas.ac.cn

© 2011 Chinese Physical Society and IOP Publishing Ltd

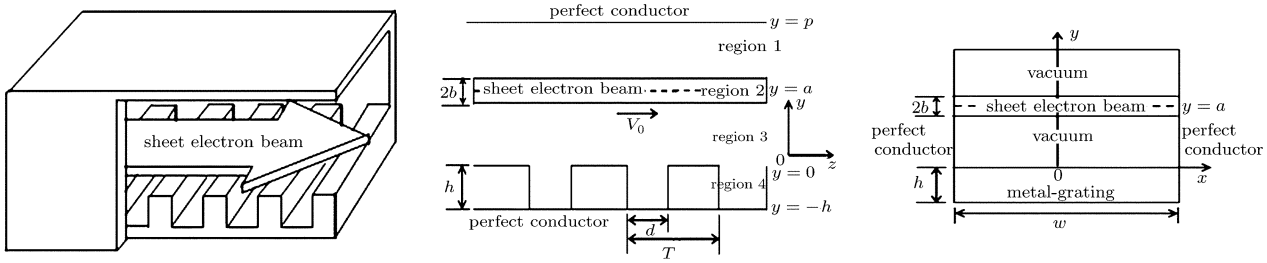
to the particle in cell (PIC) simulation, he obtained 1.2-dB/cm gain at 28.7 GHz using the sheet electron beam (140 kV, 15 A) and the interaction efficiency approached to 15%–25%. McVey *et al.*[16] dealt with a cold dispersion equation without a beam for a metal-grating rectangular waveguide structure that can be used in an RCM as an interaction circuit.[16] Mehrany and Rashidian[17] proposed a two-dimensional (2D) model of the sheet beam Cerenkov grating amplifier, in which the transverse geometrical boundaries are open.

In this paper, a three-dimensional (3D) beam-wave interaction model of the RCM is proposed, in which the transverse geometrical boundaries are closed with perfect metal. By using the field-match method at interfaces, a hybrid-mode dispersion equation and its analytical solution are derived. Through numerical calculations, the effects of the relevant electric and geometrical parameters on the linear growth rate are analysed. Moreover, the performance difference between this closed RCM and its corresponding open structure without the upper boundary is compared.

2. Model and formulas

2.1. Model

Figure 1 shows the model of the RCM with the sheet beam, which consists of a rectangular waveguide of height p and width w with periodic metal-gratings. The grating has a periodicity T, groove width d and depth h. A sheet electron beam interacts with the guided wave in the structure. The dotted line at $y = a$ corresponds to the central plane of the beam. The sheet beam is immersed in a strong axial magnetic field that constrains electron motion only along the z axis. The drift velocity of the beam v_0 is constant and the beam thickness is $2b$. All the derivations in this paper are based on this model.



(a) 3D view (b) Longitudinal section (c) Transerse section

Fig. 1. Model of RCM with sheet beam.

2.2. Derivation of dispersion equation

If the z axis is chosen as the longitudinal direction, the modes in this structure are hybrid modes that simultaneously include the z-axial field components E_z and H_z, which can be represented by the superposition of the normal TE and TM modes in a perfect metal waveguide. However, as shown in Refs. [16] and [18], the hybrid mode discussed here can be simply expressed as a transverse electric mode with respect to the x direction, TE_x.

For a self-consistent analysis, the electron motion equations and Maxwell equations must be combined to obtain a solution. As shown in Fig. 1, the whole structure can be divided into four different regions. Regions 1, 2, 3, and 4 are defined as $a + b < y < p$, $a - b < y < a + b$, $0 < y < a - b$, and $-h < y < 0$, respectively.

2.2.1. Field solutions in regions 1, 2 and 3

By linearizing Lorentz-force equations and Maxwell equations, the beam region 2 can be replaced by an equivalent dielectric layer with the effective permittivity constant as below,[18−20]

$$\varepsilon = \begin{pmatrix} 1 & 0 & 0 \\ 0 & 1 & 0 \\ 0 & 0 & 1+\chi_{\mathrm{b}} \end{pmatrix}, \tag{1}$$

where the susceptibility $\chi_{\mathrm{b}} = -\omega_{\mathrm{p}}^2/(\gamma^2(\omega - v_0\beta)^2)$ reflects the electron polarization response to the perturbing field component E_z. ω_{p}, β, and γ denote plasma frequency, propagation constant and relativistic factor, respectively. Hence the field solution can be reduced into an equivalent multilayer field problem.

By using the method of variable separation, the

field solution can be expressed as

$$H_{xi} = \sum_{n=-N}^{N} a_{in} \sin\left(k_x\left(x+\frac{w}{2}\right)\right) \times \left(\mathrm{e}^{\mathrm{j}k_{yi}y} + R_{in}\,\mathrm{e}^{-\mathrm{j}k_{yi}y}\right)\mathrm{e}^{\mathrm{j}\beta_n z}, \quad (2)$$

where $i = 1$, 2, and 3 correspond to region 1, 2, and 3 respectively; a_{in} is the amplitude coefficient; the values of R_{in}, when the values of index, i take 1, 2, and 3, respectively, denote reflection coefficients in the planes $y = p$, $y = a + b$, and $y = ab$;

$$\beta_n = \beta_0 + \frac{2n\pi}{T}, \quad k_x = \frac{l\pi}{w}, \quad l = 1, 2\ldots, \quad (3a)$$

$$k_{y1} = k_{y3} = k_y = \sqrt{k_0^2 - k_x^2 - \beta_n^2},$$

$$k_{y2} = k_{yb} = \sqrt{\frac{k_0^2\varepsilon_n - k_x^2}{k_0^2 - k_x^2}\left(k_0^2 - k_x^2 - \beta_n^2\right)} \quad (3b)$$

with

$$\varepsilon_n = \begin{cases} 1+\chi_n & \text{in region 2,} \\ 1 & \text{in regions 1 and 3,} \end{cases}$$

$$\chi_n = \frac{-\omega_{\mathrm{p}}^2}{\gamma^2(\omega - \upsilon_0\beta_n)^2}. \quad (3c)$$

By using the metallic boundary condition and the continuous conditions of the transverse fields, the reflection coefficient, R_{in}, can be obtained through tedious algebraic operations,

(i) in the plane $y = p$

$$R_{1n} = \mathrm{e}^{\mathrm{j}k_y 2p}; \quad (4a)$$

(ii) in the plane $y = a + b$

$$R_{2n} = \frac{1 - \dfrac{\mathrm{j}\,k_y \tan(k_y(a+b-p))}{k_{yb}}\dfrac{k_0^2\varepsilon_n - k_x^2}{k_0^2 - k_x^2}}{1 + \dfrac{\mathrm{j}\,k_y \tan(k_y(a+b-p))}{k_{yb}}\dfrac{k_0^2\varepsilon_n - k_x^2}{k_0^2 - k_x^2}} \times \mathrm{e}^{2\mathrm{j}k_{yb}(a+b)}; \quad (4b)$$

(iii) in the plane $y = a - b$,

$$R_{3n} = \frac{1 - \dfrac{k_0^2 - k_x^2}{k_0^2\varepsilon_n - k_x^2}\dfrac{k_{yb}}{k_y}\dfrac{\mathrm{e}^{2\mathrm{j}k_{yb}(a-b)} - R_{2n}}{\mathrm{e}^{2\mathrm{j}k_{yb}(a-b)} + R_{2n}}}{1 + \dfrac{k_0^2 - k_x^2}{k_0^2\varepsilon_n - k_x^2}\dfrac{k_{yb}}{k_y}\dfrac{\mathrm{e}^{2\mathrm{j}k_{yb}(a-b)} - R_{2n}}{\mathrm{e}^{2\mathrm{j}k_{yb}(a-b)} + R_{2n}}}\,\mathrm{e}^{2\mathrm{j}k_y(a-b)}. \quad (4c)$$

2.2.2. Field solutions in region 4

In general, the field solution in region 4 can be expanded into a Fourier series with the following form:[16,21]

$$H_x = \sum_{m=0}^{\infty} B_m \cosh\sqrt{\left(\frac{m\pi}{d}\right)^2 + k_x^2 - k_0^2}\,(y+h) \times \sin k_x\left(x+\frac{w}{2}\right)\cos\frac{m\pi}{d}z. \quad (5)$$

However, if $T \ll \lambda_0$ and the z dependence of the field quantity can be neglected, the fields in region 4 can be approximately represented by the lowest order mode in formula (5) as below

$$H_x = B_0 \sin k_x\left(x+\frac{w}{2}\right)\cosh\sqrt{k_x^2 - k_0^2}\,(y+h), \quad (6a)$$

$$E_z = \frac{-\mathrm{j}\,\omega\mu B_0\sqrt{k_x^2 - k_0^2}}{k_0^2 - k_x^2}\sin k_x\left(x+\frac{w}{2}\right) \times \sinh\sqrt{k_x^2 - k_0^2}\,(y+h). \quad (6b)$$

Subsequently, the approximate continuous conditions of the tangent field components at $y = 0$ are applied

$$E_{z3}(x, 0^+, z) = \begin{cases} E_{z4}(x, 0^-, z), & 0 < z < d, \\ 0, & d < z < T, \end{cases} \quad (7a)$$

$$H_{x3}(x, 0^+, z) = H_{x4}(x, 0^-, z). \quad (7b)$$

Through algebraic operations, a simplified dispersion equation can be written as

$$D(\beta_0, \chi) = \sum_{n=-N}^{N} \frac{\sin c^2\left(\beta_n\dfrac{d}{2}\right)}{\mathrm{j}\,k_y}\frac{1+R_{3n}}{1-R_{3n}} - \frac{T\coth\sqrt{k_x^2 - k_0^2}h}{d\sqrt{k_x^2 - k_0^2}} = 0. \quad (8)$$

As the beam density approaches to zero, there exist the following relationships:

$$\varepsilon_n \to 1, \quad (9a)$$

$$R_{3n} \to \mathrm{e}^{\mathrm{j}\,k_y 2p}, \quad (9b)$$

$$\frac{1+R_{3n}}{1-R_{3n}} \to \frac{-1}{\tanh(\mathrm{j}k_y p)}. \quad (9c)$$

Hence, equation (8) can be reduced into

$$\sum_{n=-N}^{N} \frac{\sin c^2\left(\beta_n\dfrac{d}{2}\right)}{k_y \tanh(\mathrm{j}\,k_y p)} = \frac{\cot\left(\mathrm{j}\sqrt{k_x^2 - k_0^2}h\right)}{\sqrt{k_x^2 - k_0^2}}\frac{T}{d}. \quad (10)$$

Equation (10) is consistent with the cold dispersion equation obtained in Ref. [16].

2.2.3. Analytical solution of dispersion equation

Usually, one can obtain the complex propagation constant by solving the transcendental Eq. (8) numerically. However, when the dilute beam assumption is adopted, an approximate solution can be obtained. There are the guided surface-wave and the space-charge wave in the RCM with sheet beam. According to the coupling mode theory, the coupling between the two waves becomes strong when their phase velocities are close to each other, which is commonly known as the synchronous condition. The coupled fields are modified from the fields of an uncoupled guided surface-wave. Since the beam is dilute (i.e. $\chi_{\rm b} \ll 1$), the field modification due to the coupling is moderate. Based on this point, equation (8) can be expanded around $\chi_{\rm b} = 0$ and the resonant point $(\omega_{\rm res}, \beta_{\rm res})$ using Taylor series,

$$\begin{aligned} D(\omega,\beta,\chi) = {} & D(\omega,\beta,\chi_{+1})\,\big|_{(\omega_{\rm res},\beta_{\rm res},\chi=0)} \\ & + \delta\beta \frac{\partial D(\chi_{+1}=0)}{\partial\beta}\,\big|_{(\omega_{\rm res},\beta_{\rm res})} \\ & + \chi_{+1}\frac{\partial D}{\partial\chi_{+1}}\,\big|_{(\omega_{\rm res},\beta_{\rm res},\chi=0)}\,. \end{aligned} \tag{11}$$

If the first harmonic of the guided surface wave strongly couples to the space-charge wave, the propagation constant can be written as

$$\beta_0 = \omega/\nu_0 - 2\pi/T + \delta\beta. \tag{12}$$

Through combining Eqs. (3a), (3c), and (12), the first-order susceptibility χ_{+1} can be expressed as

$$\chi_{+1} = -\frac{(\omega_{\rm p}/\gamma)^2}{(\delta\beta\nu_0)^2}. \tag{13}$$

Substituting Eq. (13) into Eq. (11), one can obtain

$$\delta\beta = \left[\frac{(\omega_{\rm p}/\gamma)^2\,\dfrac{1}{v_o^2}\dfrac{\partial D\,(\beta_0,\chi_{+1})}{\partial\chi_{+1}}}{\dfrac{\partial D\,(\beta_0,\chi_{+1})}{\partial\beta_0}}\right]^{1/3}. \tag{14}$$

The partial derivatives in Eq. (14) are given by

$$\begin{aligned} & \frac{\partial D\,(\beta_0,\chi_{+1})}{\partial\chi_{+1}}\bigg|_{{\rm res},\chi=0} \\ & = \left(\frac{1}{k_y}\sin c^2\left(\frac{\omega}{v_0}\frac{d}{2}\right)\frac{2}{(1-R_{31})^2}\frac{\partial R_{31}}{\partial\varepsilon}\right)\bigg|_{{\rm res},\chi=0}, \end{aligned} \tag{15}$$

where

$$\begin{aligned} \frac{\partial R_{31}}{\partial\varepsilon} = {} & \frac{{\rm e}^{2{\rm j}k_y(a-b)}}{\left(1+\dfrac{{\rm e}^{2{\rm j}k_{yb}(a-b)}-R_{21}}{{\rm e}^{2{\rm j}k_{yb}(a-b)}+R_{21}}\right)^2} \\ & \times\left[-2\psi+\frac{{\rm e}^{2{\rm j}k_{yb}(a-b)}-R_{21}}{{\rm e}^{2{\rm j}k_{yb}(a-b)}+R_{21}}\frac{k_0^2}{k_0^2-k_x^2}\right], \\ R_{21} = {} & \frac{1-{\rm j}\,\tan k_y(a+b-p)}{1+{\rm j}\,\tan k_y(a+b-p)}\,{\rm e}^{2{\rm j}k_y(a+b)}, \end{aligned}$$

$$\psi = \frac{{\rm j}2k_0^2}{k_0^2-k_x^2}\frac{1}{({\rm e}^{-2b{\rm j}\,k_{yb}}+{\rm e}^{2a{\rm j}\,k_y})^2}\left[-2b\sqrt{k_0^2-k_x^2-\left(\frac{\omega}{v_0}\right)^2}\frac{1-{\rm j}\,\tan k_y(a+b-p)}{1+{\rm j}\,\tan k_y(a+b-p)}+\frac{\tan k_y(a+b-p)}{(1+{\rm j}\,\tan k_y(a+b-p))^2}\right],$$

$$\begin{aligned} & \frac{\partial D\,(\beta_0,\chi=0)}{\partial\beta_0} \\ & = \sum_{n=-N}^{N}\frac{1+R_{3n}}{1-R_{3n}}\frac{d\sin c(\beta_n d/2)}{k_y}\frac{\dfrac{\beta_n d}{2}\cos\left(\dfrac{\beta_n d}{2}\right)-\sin\left(\dfrac{\beta_n d}{2}\right)}{(\beta_n d/2)^2}+\sum_{n=-N}^{N}\frac{1+R_{3n}}{1-R_{3n}}\frac{\beta_n\sin c^2(\beta_n d/2)}{k_y^2\sqrt{k_0^2-k_x^2-\beta_n^2}} \\ & + \sum_{n=-N}^{N}\frac{-8a{\rm j}\,\beta_n}{k_y\,(1-R_{3n})^2}\frac{\sin c^2\dfrac{\beta_n d}{2}(1-{\rm j}\,\tan k_y(a+b-p))\,{\rm e}^{2{\rm j}k_{yb}(a+b)}}{(1+{\rm j}\,\tan k_y(a+b-p))\sqrt{k_0^2-k_x^2-\beta_n^2}}. \end{aligned} \tag{16}$$

According to Eq. (12), the linear growth rate is the imaginary part of Eq. (14).

3. Numerical calculation

As an example, a sheet beam interacting with the first harmonic of the $\rm TE_{x10}$ mode in the RCM is investigated by the linear theory. The propagation constant of the uncoupled guided wave is $\beta_0 = 915/{\rm m}$. The waveguide-grating parameters used in the calculation for the RCM are listed in Table 1.

Table 1. Waveguide-grating parameters.

Parameters	Closed RCM
Grating periodicity T/mm	1.8
Grating width d/mm	0.8
Grating depth h/mm	6
Waveguide height p/mm	7.9
Waveguide width w/mm	15.8
Beam thickness $2b$/mm	2.2
Beam central position a/mm	2.1

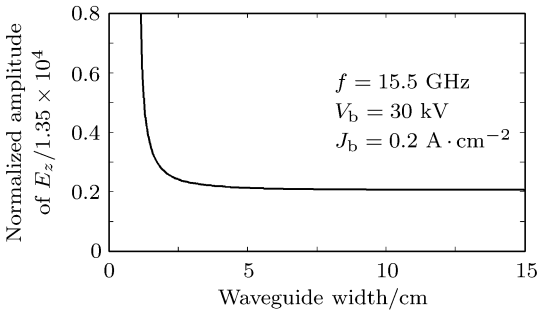


Fig. 2. Normalized amplitude of longitudinal field component E_z versus waveguide width.

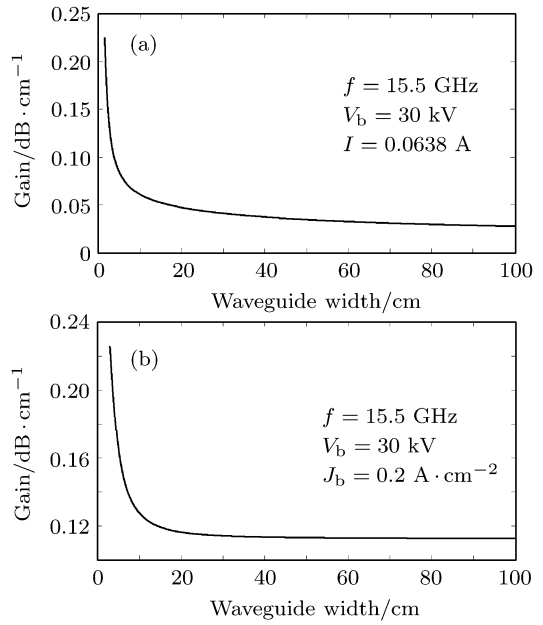


Fig. 3. Gains versus waveguide width (a) for a total current of 0.0638 A, and (b) for a current density of 0.2 A/cm2.

Figure 2 shows that the normalized amplitude of the longitudinal field component E_z falls quickly with the increase of waveguide width when the width is less than 5 cm and gradually reaches a stable value with the further increase of the width. This implies that the coupling between the beam and the guided wave weakens as width increases. The same initial state is used in Figs. 3(a) and 3(b), in which the initial value of the current density and the total current are 0.2 A/cm^2 and 0.0638 A, respectively. Moreover, the total current keeps invariant in Fig. 3(a) and the current density is invariant in Fig. 3(b). Figure 3(a) exhibits the gains versus the waveguide width for the total current of 0.0638 A, which shows that the gain drops off markedly with the increase of waveguide width when the width is less than 5 cm and gradually approaches a stable value with the further increase of the width. Based on the model in Fig. 1, it can be seen that beam region 2 is broadened as the waveguide width increases, which leads to the reduction of the current density because the total current is invariant. Moreover, as shown in Fig. 2, the normalized amplitude of the E_z also drops off with the increase of waveguide width. Hence it is the decreasing current density and the reduced amplitude of the E_z that result in the descending of the gain with the increase of waveguide width as shown in Fig. 3(a). In Fig. 3(b), the gain decreases significantly with the increase of waveguide width when the width is less than 5 cm and gradually trends to the stable value with the further increase of the width. It should be noted that the total current is enhanced to keep the constant current density. However, even the current density is invariant, the decrease in amplitude of the E_z (Fig. 2) will cause the reduction in gain when the width is less than 5 cm, as shown in Fig. 3(b).

Figure 4 illustrates the effects of beam thickness and beam-grating gap (the distance between the beam and the metal grating) on linear growth rate for the current density being 0.2 A/cm^2. The solid line in Fig. 4 is for the approximate solution from Eq. (14), and the dashed line is for the numerical solution obtained from Eq. (8). Figure 4(a) exhibits the gain versus the beam thickness with a beam grating gap of 1 mm, which shows that the gain grows rapidly when the beam thickness is less than 1 mm, this growth slows down after the thickness is over 1 mm and the gain gradually trends to saturation with the further increase of the thickness. This can be explained by the fact that the beam shields the evanescent tail of the guided waves. Figure 4(b) indicates that the gain decreases with the increase of the beam grating gap for a beam thickness of 4 mm. The increase of the gap in fact causes the weakening of the coupling between the guided surface-wave and the space-charge

wave. In addition, the gain almost keeps constant for a beam grating gap in a range of 1 mm–1.4 mm, which may be helpful for the beam–wave interaction in the RCM.

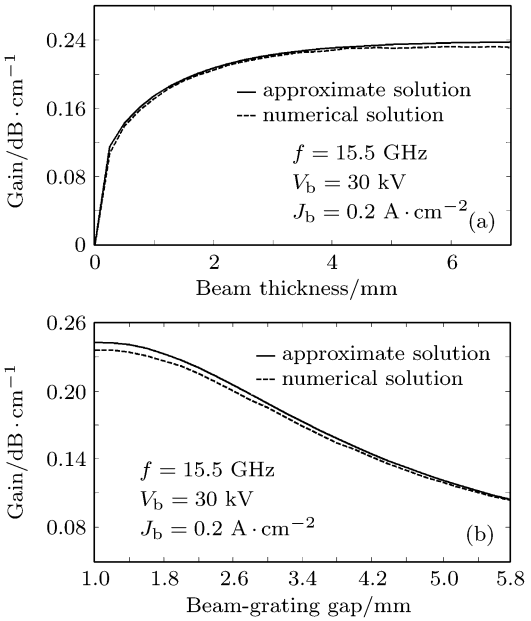


Fig. 4. Gains versus beam thickness (a) and beam grating gap (b).

Figure 5 exhibits the gain versus current density, which shows that the gain rises with the increase of the current density for the given structural parameters and working frequency. It should be noted that this rise is nearly linear if the current density is large enough and $\chi_b \ll 1$. In Fig. 6, the gain quickly rises with the increase of the beam voltage when the voltage is less than 55 kV and the gain is not sensitive to the variation of the voltage near 55 kV, and then gradually falls when the voltage is larger than 60 kV. This implies that the synchronism condition for the beam-wave interaction is satisfied well near the beam voltage of 55 kV, which corresponds to the maximum linear growth rate of 0.465 dB/cm at a frequency of 15.5 GHz and a current density of 0.1 A/cm^2.

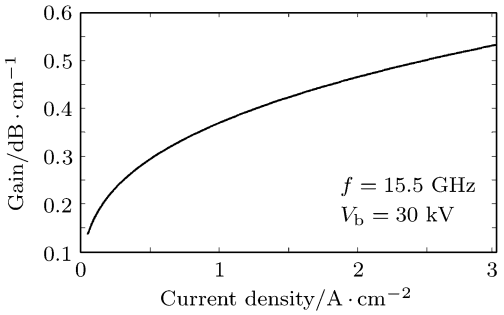


Fig. 5. Gain versus current density.

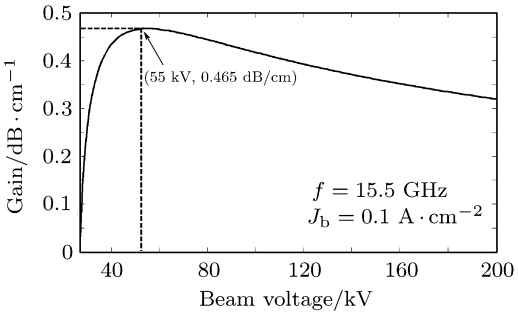


Fig. 6. Gain versus beam voltage.

The longitudinal electric field profile and the linear growth rate in the RCM for the closed transverse geometrical boundaries are compared with those in the RCM for a corresponding open structure without the upper boundary in Figs. 7 and 8. The waveguide width is selected to be 250 mm in this case, much larger than the height of the waveguide, so the effect of the waveguide width on linear growth rate can be neglected. Based on this point, the influence of the upper boundary on linear growth rate can be investigated in detail. The other structural parameters employed in Figs. 7 and 8 are listed in Table 1. As shown in Fig. 7, the field component E_z shows an evanescent distribution along the y direction, and the normalized amplitude of the field in the closed RCM is greater than that in the open structure when y is less than 6.4. However, the field component E_z in the closed RCM must vanish at $y = 7.9$ to satisfy the metallic boundary condition, which leads to a faster decrease of the curve in the region $y > 6.4$. Figure 8 shows that the gain in the RCM with closed transverse geometrical boundaries is significantly larger than that in the corresponding open structure when the beam-grating gap is in a range of 1 mm–5 mm. In fact, the outward radiation of the transmitted power can be constrained by the upper boundary in the RCM, which results in the higher amplitude of the E_z as well as the stronger coupling between the beam and the guided wave.

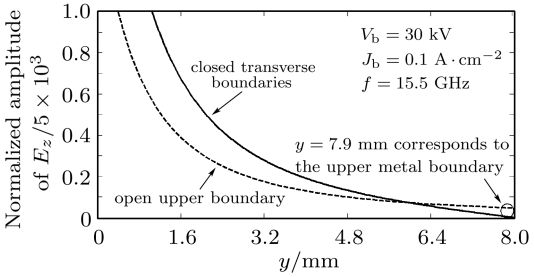


Fig. 7. Normalized amplitude of longitudinal field component E_z versus y.

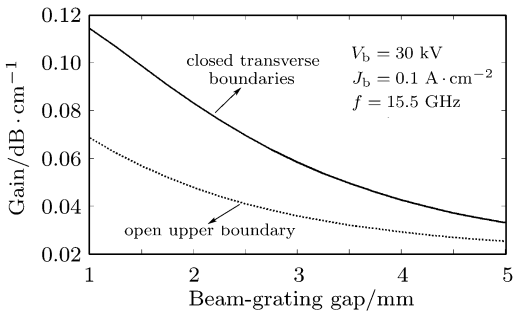


Fig. 8. Gain versus beam-grating gap.

4. Conclusion

In this paper, a 3D beam–wave interaction model of the RCM with a sheet beam is proposed. The dispersion equation in the RCM is derived by solving an equivalent multilayer field problem for the sheet beam linearly interacting with the hybrid modes. Moreover, the linear growth rate in the synchronism regime is investigated under the condition of the low current density limit ($\chi_b \ll 1$). The effects of the main working parameters on the linear growth rate are analysed through numerical calculations. The results show that for this RCM, the closed transverse boundary avoids the effect of RF radiation on linear growth rate and a linear growth rate of 0.465 dB/cm can be reached at a beam voltage of 55 kV, a current density of 0.1 A/cm^2 and a frequency of 15.5 GHz. In addition, the gain almost keeps constant for a beam grating gap in a range of 1 mm–1.4 mm, which may be helpful for beam–wave interaction in the RCM.

References

[1] Walsh J E, Marshall T C and Schlesinger S P 1977 *Phys. Fluids* **20** 709

[2] Felch K L, Busby K O, Layman R W, Kapilow D and Walsh J E 1981 *Appl. Phys. Lett.* **38** 601

[3] Laven S V, Branscum J, Golub J, Layman R and Walsh J E 1982 *Appl. Phys. Lett.* **41** 408

[4] Garate E P, Moustaizis S, Buzzi J M, Rouille C and Lamain H 1986 *Appl. Phys. Lett.* **48** 1326

[5] Walsh J E, Shaughnessy C H, Layman R, Dattoli G, Gallerano G P and Renieri A 1988 *Nucl. Instr. Method* A **272** 132

[6] Garate E, Kosai H, Evans K, Fisher A, Cherry R and Main W 1990 *Appl. Phys. Lett.* **56** 1092

[7] Kosai H, Garate E, Fisher A and Main W 1992 *IEEE Trans. Plasma Sci.* **20** 288

[8] Zhao D, Ding Y, Wang Y and Ruan C 2010 *Phys. Plasmas* **17** 113110

[9] He J, Wei Y, Gong Y, Duan Z and Wang W 2010 *Acta Phys. Sin.* **59** 2843 (in Chinese)

[10] Zhang J, Zhong H, Shu T and Yang J 2003 *Chin. Phys. Lett.* **20** 2265

[11] Kuzelev M V, Rukhadze A A and Strelkov P S 1987 *Sov. J. Plasma Phys.* **13** 793

[12] Carmel Y, Minami K and Weiran J 1990 *IEEE Trans. Plasma Sci.* **18** 497

[13] Kosai H, Garate E and Fisher A 1990 *Proc. SPIE* **1226** 191

[14] Sheng-Fuh R C, Scharer J E and Booske J H 1992 *IEEE Trans. Plasma Sci.* **20** 293

[15] Carlsten B E 2002 *Phys. Plasmas* **9** 1790

[16] McVey B D, Basten M A, Booske J H, Joe J and Scharer J E 1994 *IEEE Trans. Microwave Theory and Techniques* **42** 995

[17] Mehrany K and Rashidian B 2003 *IEEE Trans. Electron Dev.* **50** 1562

[18] Hu Y, Yang Z, Li B, Li J, Huang T, Jin X, Zhu X and Liang X 2010 *Acta Phys. Sin.* **59** 5439 (in Chinese)

[19] Lawson J D 1988 *The Physics of Charged Particles* Chap. 6 (Oxford: Clarendon) p. 293; see also, Joe J, Chang S F, Scharer J and Booske J 1991 *Microwave Opt. Technol. Lett.* **4** 443

[20] Peng W, Hu Y, Yang Z, Li J, Lu Q and Li B 2010 *Acta Phys. Sin.* **59** 8478 (in Chinese)

[21] Zhang K and Li D 2001 *Electromagnetic Theory for Microwaves and Optoelectronics* (Beijing: Electronics Industry Press) (in Chinese)